*MRS Communications*
© The Author(s) 2022
https://doi.org/10.1557/s43579-022-00244-y

MRS Communications

Research Letter

# Examining the inherent strains of aluminium alloy 7050-T7451 powder for additive manufacturing processes

**Ramona Dogea, and Xiu T. Yan,** Department of Design, Manufacture and Engineering Management (DMEM), University of Strathclyde, Glasgow, Scotland
**Richard Millar,** National Manufacturing Institute Scotland – University of Strathclyde, Glasgow, Scotland

Address all correspondence to Ramona Dogea at **ramona.dogea@strath.ac.uk**

(Received 20 June 2022; accepted 16 August 2022)

## Abstract

Aluminium alloys (AA) are ubiquitous materials in manufacturing used in powder bed fusion (PBF) processes due to light weight, high strength and corrosion resistance. Current research focuses on other materials whilst additively manufactured AA 7050 remains unexplored. This paper examines the formability of AA 7050-T7451 powder for the Selective Laser Melting (SLM) process. To define this material in Simufact AdditiveTM the creep behaviour required flow curves obtained by writing a MATLAB® script to calculate the true stress–strain behaviour depending on strain rate and temperature. The results of the mechanical calibration for aluminium alloy are presented to obtain its inherent strains.

## Introduction

Additive manufacturing (AM) is being actively explored for use in aerospace when fabricating structural components to create possibilities for adding value to the product compared to traditional manufacturing processes. The advantages of using additive manufacturing for aerospace components are the reduced lead time and the associated costs, the ability to design and manufacture complex lightweight geometries, while improving their performance compared to conventional manufacturing. AM has the capability for manufacturing replacement parts faster than other processes, and it can offer other performance features such as localised heat treatments, surface hardening or alloying, material removal, part repair, and high-performance prototype parts.[1] One major criterion to consider when selecting a particular type of AM is the choice of appropriate materials. These prerequisites for material selection are mostly dependent on their attained performance in service, their processing tendencies for optimising the required geometries and properties, and their ability to produce feedstock effectively, amongst others. Different materials including polymers, ceramics, metals and their composites are applied to a particular AM technique depending on the AM manufacturability index.[2] In particular, polymers and their composites, such as the polyether ketone (PEK) are adopted in aerospace and aeronautical applications due to their high load-bearing capacity, excellent chemical resistance and thermal stability. Others, like the polyether ketone ketone (PEKK) are also adopted in the aerospace sector due to their generally good properties, their low shrinkage and high powder usability rate which makes them a potentially high-performance type of material for selective laser sintering.[3] For this research 7050-T7451 aluminium alloy was selected since it was used at the part design stage[4] and it will be used in the next stage to manufacture a wing rib. This alloy is heat treatable and used in various aerospace applications including wing skins, bulkheads and fuselage frames, and it is a popular commercial alloy in the aerospace industry.[5] The numerical simulations of AM processes have tried to reproduce the manufacturing process in a way similar to the industrial practices. The most suitable numerical method for coping with the simulation of the SLM process is based on the Inherent Strain approach. This enables a fast prediction of the distortions and the residual stresses of the manufactured part, assuming the general hypothesis widely accepted in Computational Welding Mechanics.[6] But the fully coupled transient thermo-mechanical analysis is replaced by a layer-by-layer sequence of steady-state mechanical analysis. Each new layer is created with an initial displacement field influenced by the movements of the shared nodes with the previous active elements. Hence, the newly activated strain field is induced by the initial displacements. If the simulation does not remove this computation, the entire solution will be affected by a pre-stress field.[7] A typical layer thickness of 0.08–0.15 mm is used for PBF, whilst for DED it is 0.089–0.203 mm.[8] In the context of AM process, formability of a material is critical to understand how a material behaviour in the AM process. Formability of a material is therefore defined as an attribute of a power material in terms how easy to generate an accurate printed part during the printing process. It considers inherent strain along X, Y and Z axis as a key measurement, heat dissertation and layer thickness, amongst others.

Due to the local heat input during the manufacturing process, the component does not cool homogeneously and thermal gradients are introduced.[9] One of the biggest limitations of conventional methods of manufacturing using Al 7xxx alloys is hot tearing, which is very common when casting this series of aluminium alloys. Controlled diffusion solidification

(CDS) was proposed to avoid hot tearing.[10] In addition, the increase of the zinc content leads to higher hot tearing susceptibility.[11] To perform stress correction the inherent strain calibration approach is usually used in the virtual simulation of AM processes. Possible correction strategies are based on the octree refinement strategy. This refines specific areas of interest that are comprised within certain nodes. Also, there is the adaptive finite element approach, which estimates the discretisation errors and the refinement of finite element models, and finally there is stress correction caused by inherent strains.[7] In Simufact Additive™ a mechanical calibration is required to estimate the inherent stress values of the material before a simulation is performed. The inherent strain results from thermal strain, plastic strain and phase transformations, that also depend on material properties and process parameters[8]:

$$\varepsilon^{inherent} = \varepsilon^{th} + \varepsilon^{pl} + \varepsilon^{ph} \quad (1)$$

The calibration process can be done through experiments or simulations. Alzyod and Ficzere used simulations of two cantilevers for the calibration process in Simufact Additive™ for TiAl6V4, AlSi10Mg and 316L.[8] The two cantilever geometries are already predefined and located on the X- and Y-axis perpendicular to each other. The maximum distortion on the Z-axis is measured and the values of the inherent strains in the three directions X, Y and Z are estimated. Stress relief is usually simulated using a creep model that is obtained empirically. Creep describes the time and temperature dependent plastic deformation at certain at constant load/stress or constant elongation/strain conditions. Creep helps to decrease the residual stresses by transforming them into plastic deformation. Its properties are needed to simulate appropriate stress relief during heat treatment and hot isostatic pressing (HIP) processes in Simufact Additive™. In addition, an added difficulty is the limited availability of creep data for materials manufactured using PBF.[12] One model for the strain rate equation is given in[13]:

$$\dot{\varepsilon} = \frac{d\varepsilon}{dt} = A[sinh(\alpha\sigma)]^n e^{\left(-\frac{Q}{RT}\right)} \quad (2)$$

where $A$ is a constant related to material microstructure; $\alpha$ is a material constant in $Pa^{-1}$; $\sigma$ is the applied stress, in Pa; $n$ is the stress exponent; $Q$ is the deformation activation energy, in $J \cdot mol^{-1}$; $R$ is the gas constant, equal to 8.3145 $J \cdot mol^{-1} \cdot K^{-1}$; $T$ is the temperature, in K. Current research shows the difficulty to select the parameters for the strain rate equation since they strongly depend on pre-strained conditions. For the aluminium alloy 7050, the stress exponent remains unchanged with initial stress levels, but it increases with pre-strained stress levels, ranging from 3.1 to 3.5.[14] For pure aluminium, the deformation activation energy is 142 kJ/mol[15] while typical values for aluminium alloys are 124 kJ/mol for a 5%-Zn alloy, 134 kJ/mol for Al 7475, and 119 kJ/mol for Al–Zn–Mg–Cu alloys.[16] For AA7050-T7451 aluminium alloy, Sang et al. obtained the constants experimentally depending on three deformation modes: hot tensile, hot compression, and hot shear compression.[13]

The flow behaviour of aluminium alloy 7050 has been already ifnvestigated and its true stress–strain curves, also known as flow curves, have been obtained. Chen et al. performed some experiments to get the flow curves for temperatures between 20°C and 270°C for a wide range of strain rates: 0.0001, 0.01, 2500, 4000, 7500 and 10,000 $s^{-1}$. Besides this they were also able to derive a mathematical model using statistical analysis.[17] In this work, the true stress–strain equation will be used to calculate the strain rates 0.001, 0.01, 0.1, and 1 $s^{-1}$ for Simufact Additive™ flow curves input. In the work done by Liu et. al., the flow curves of the water-quenched and furnace-cooled specimens deformed at 300°C, 350°C, 400°C and 450°C are represented for four different strain rates: 0.001, 0.01, 0.1, and 1 $s^{-1}$, but not for temperatures lower than 300°C.[18] In this work, their flow curves of the water-quenched specimens will be modelled for Simufact Additive™ simulations. Li et al.obtained experimentally the flow curves for AA7050 at 573, 623, 673 and 723 K at the strain rates 0.001, 0.01, 0.1, and 1 $s^{-1}$.[19] These curves will be also modelled for this work to define the AA7050-T7451 in Simufact Additive™.

Current research is focused on Ti-6Al-4 V, Al-Si-10 Mg, 316L, 17–4 PH, and IN625,[1] while the additively manufactured 7050 aluminium alloy using SLM is still an unexplored area and it needs to be investigated.[20] For AA7050-T7451 the flow behaviour at the strain rates 0.001, 0.01, 0.1, and 1 $s^{-1}$ at low temperatures between 20°C and 270°C was modelled using a MATLAB® script that was written considering the true stress–strain equation due to the gap in the literature. To perform simulations in Simufact Additive™ with AA7050-T7451 the inherent strains are needed. For this, the mechanical calibration for this aluminium alloy was carried out considering layer thicknesses of 0.08, 0.12 and 0.15 mm, and a voxel mesh size between 0.5 and 3.5 mm. The outcomes are presented in the results and discussion section.

This work is structured into the following sections: introduction, materials and methods, results and discussion, conclusions and further work, and references.

## Materials and methods

Since the material properties for aluminium alloy AA7050-T7451 powder were not readily available, its mechanical properties and chemical composition were needed to define the material. They were introduced considering.[21]. In addition, fifty-six flow curves were introduced in Simufact Additive™ to model a wide range of temperatures for the heat treatment process considering the current research. To model the true stress–strain curves of 7050 aluminium alloy, fourteen temperature values (20°C, 50°C, 100°C, 150°C, 200°C, 270°C, 300°C,

350°C, 400°C, 450°C, 573°C, 623°C, 673°C, 723°C) at four strain rate values (0.001, 0.01, 0.1, 1 $s^{-1}$) were used.

The curves that correspond to the lower temperatures (20°C, 50°C, 100°C, 200°C and 270°C) were calculated using a MATLAB® script that was written specifically for this and which considered the true stress–strain equation. Figure 1 shows the flowchart that describes the followed methodology.

The output curves from the MATLAB® script are shown in Fig. 2.

The creep law was modelled in accordance with a hyperbolic equation as follows:

$$\dot{\varepsilon} = \frac{d\varepsilon}{dt} = 1.27 \times 10^{20} \left[ sinh\left( 0.0051 \, \frac{1}{MPa} \sigma \right) \right]^{8.05} e^{\left( -\frac{241380 \, \frac{J}{mol}}{8.3145 \, \frac{J}{molK} \, T} \right)} \quad (3)$$

The constants were selected for the hot tensile deformation mode since they are suitable to analyse the effects of heat and strain on material properties and tensile strength.

## Results and discussion

MSC Simufact Additive™ is a commercial software developed especially for powder bed fusion (PBF) additive manufacturing simulations. It allows the analysis of four techniques: selective laser melting (SLM), electron beam melting (EBM), laser beam melting (LBM), and direct metal laser sintering (DMLS). The software Simufact Additive™ also provides standard inherent strain values: $\varepsilon_{xx} = -0.008$ (X axis), $\varepsilon_{yy} = -0.003$ (Y axis), $\varepsilon_{zz} = -0.03$ (Z axis). To obtain the inherent strains that correspond to a specific material, in this case AA7050-T7451, the inherent strain calibration function in Simufact Additive™ was used. The mechanical calibration of two cantilevers was carried out for AA7050-T7451 powder to calculate the inherent strains by measuring the Z-displacement at two measuring points, one for each cantilever. For the calibration, these measuring points are needed for each part to track the distortion after cutting the specimen.

Simufact Additive™ requires as input one measuring point for each cantilever. For the calibrations, the target values of 3.09 and 2.01 mm will be taken as the Simufact Additive™ tutorial recommends.

Figure 3 shows the location of the measuring points at the two cantilevers, as well as the simulation of mechanical orthotropic calibration. After the simulation, a colour mapped geometry represents the displacements of the cantilevers.

In order to understand the impact of the printing layer sizes on the inherent strain of these cantilevers, three different layer thickness were investigated: 0.08, 0.12 and 0.15 mm. For each layer thickness, five voxel mesh sizes were simulated to ensure the consistency in computational errors during simulation. The simulations show that $\varepsilon_{zz}$ do not depend on the layer thickness. There is a slight difference for $\varepsilon_{xx}$ and $\varepsilon_{yy}$ with a voxel mesh of 3.5 mm between the layer thickness of 0.08 mm, the layer thickness of 0.12 mm and the thickness of 0.15 mm. For the X

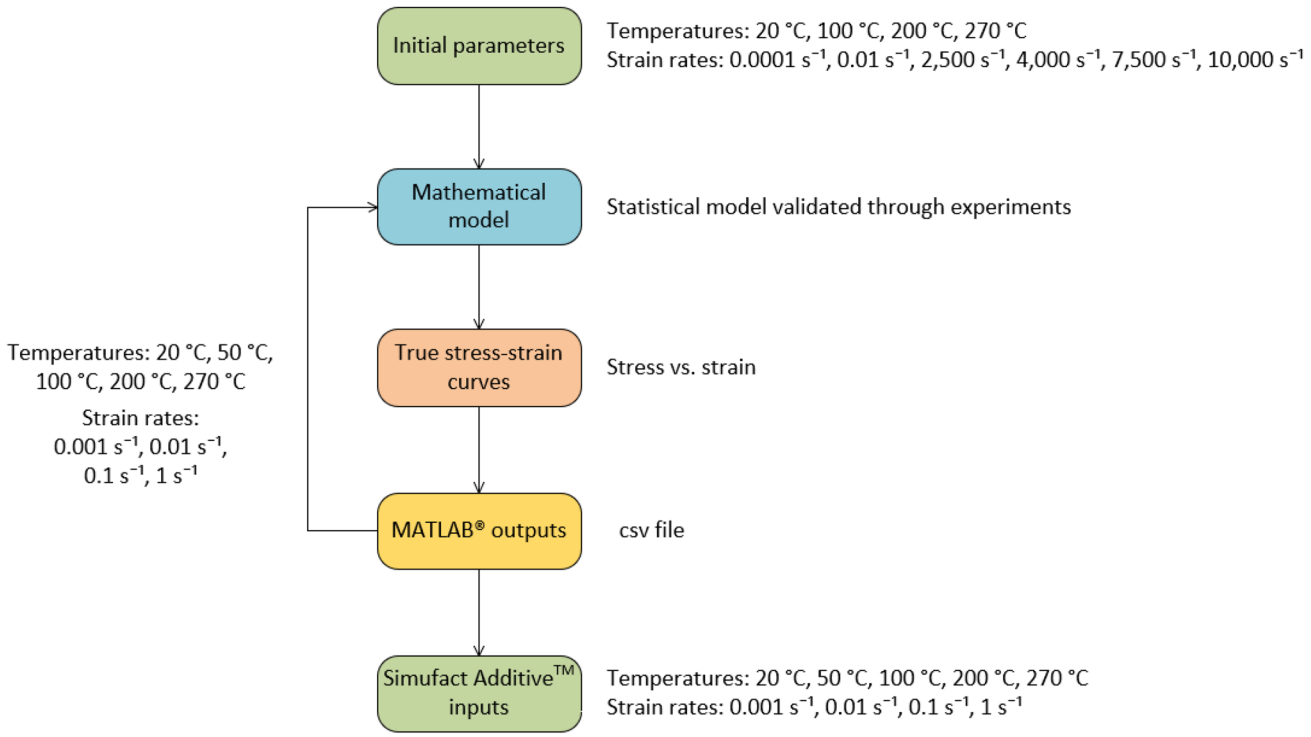


**Figure 1.** Flowchart of the MATLAB® computation.

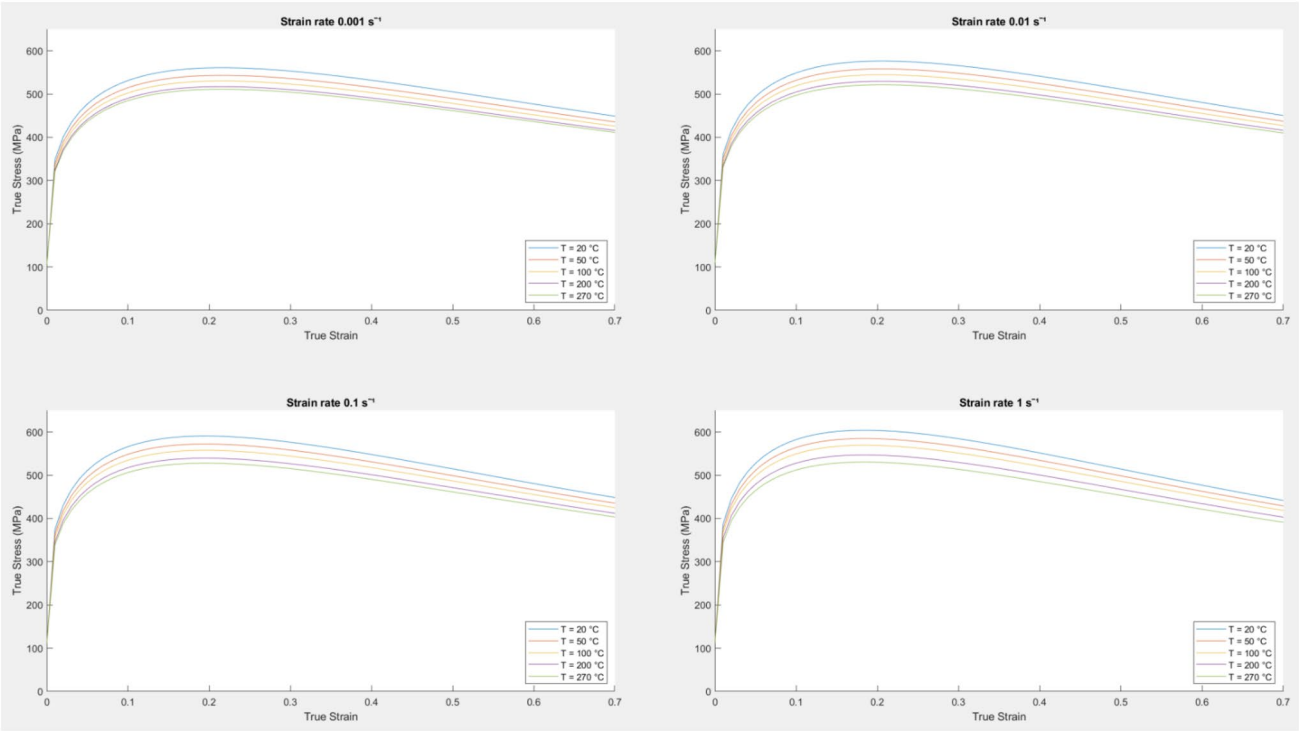


**Figure 2.** Flow curves for AA7050-T7451 at 20°C, 50°C, 100°C, 200°C and 270°C for strain rates 0.001, 0.01, 0.1, and 1 $s^{-1}$.

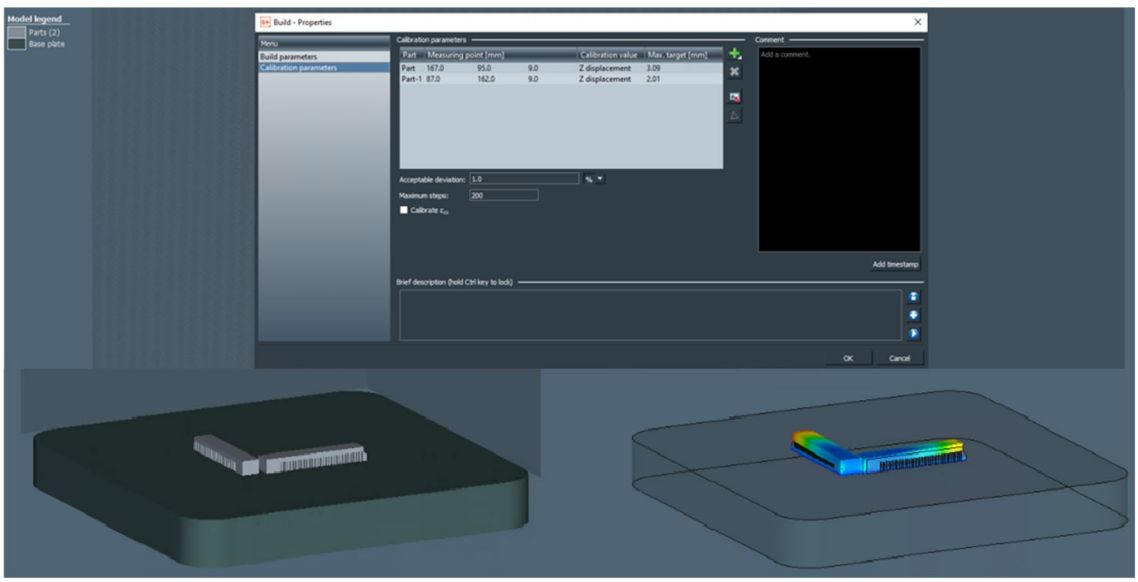


**Figure 3.** Location of measuring points at the two cantilevers (top); Simulation of mechanical orthotropic calibration using cantilevers in Simufact Additive. Bottom left: before simulation; bottom right: after simulation.

axis, the deviation is 0.1%, while in the Y axis it is 0.16%. They may be caused by the iteration process and can be neglected.

The inherent strain in the X direction $\varepsilon_{xx}$ shows a clear pattern: the finer the voxel mesh is, the smaller $\varepsilon_{xx}$ gets. In the Y direction, $\varepsilon_{yy}$ oscillates and no tendency can be recognised. In the Z direction, $\varepsilon_{zz}$ remains constant since the calibration was completed for a constant height in the x–y plane (Fig. 4).

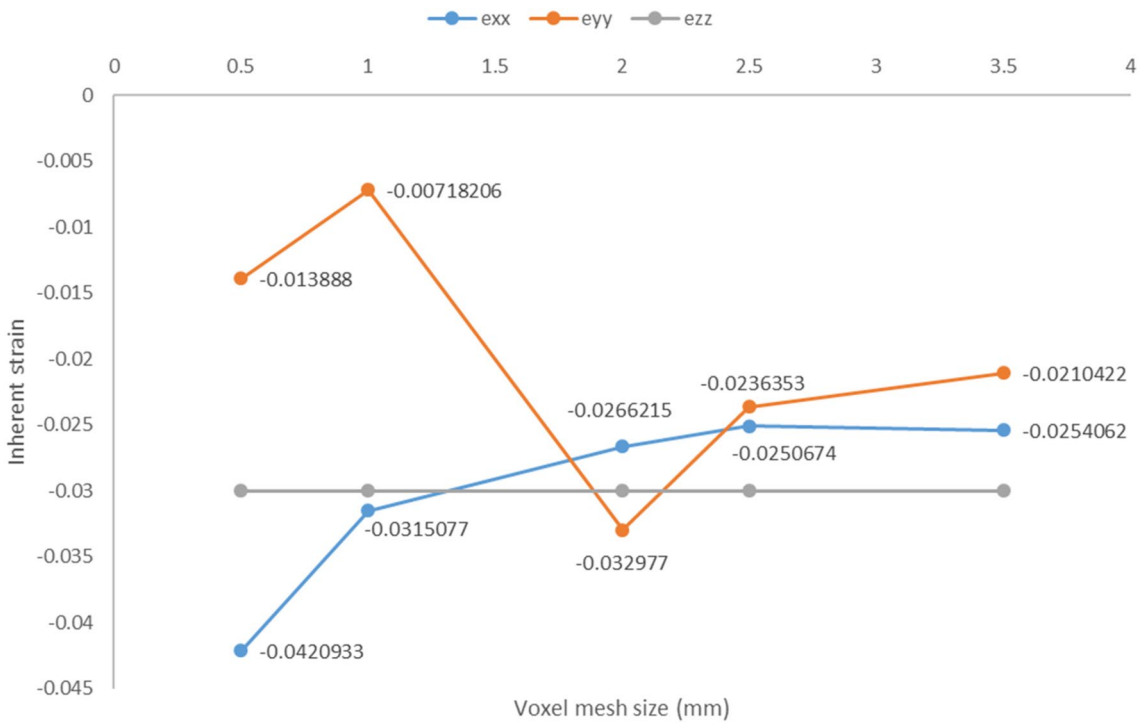


**Figure 4.** Mechanical calibration of two cantilevers: inherent strain vs. voxel mesh.

## Conclusions and future work

The aim of this paper was to investigate the formability of AA7050-T7451 powder for additive manufacturing processes. The results presented the flow curves at different strain rates and temperatures that are required for simulating parts in AM processes using Simufact Additive™. In addition, the inherent strains for this aluminium alloy powder were determined through the mechanical calibration function in Simufact Additive™. The influence of layer thickness and voxel mesh size on the inherent strains was investigated. The inherent strains do not depend on the layer thickness that were used for building the cantilevers. The finer the voxel mesh size the X axis is, the smaller $\varepsilon_{xx}$ gets. In the Y direction, $\varepsilon_{yy}$ did not show any clear phenomenological tendencies, whilst in the Z direction $\varepsilon_{zz}$ remains constant since the calibration was undertaken for a constant height in the X–Y plane. The outcomes of this work will be used in the next stage in which the additive manufacturability of an aircraft wing rib will be simulated.

Future work will deal with the re-design of the manufacturing process for an aircraft wing rib using AA7050-T7451 in a selective laser melting process in Simufact Additive™. Furthermore, it is recommended that experimental trials should be performed for AA7050-T7451 to check its microstructure, since this has become a significant research field.

## Acknowledgments

The authors acknowledge the support of the National Manufacturing Institute Scotland and the Department of Design, Manufacturing and Engineering Management of the University of Strathclyde, United Kingdom.

## Author contributions

Conceptualization, RD; methodology, RD; software, RD; validation, RD; formal analysis, XTY, RM and RD; investigation, RD; resources, RD; data curation, RD; writing—original draft preparation, RD; writing—review and editing, XTY and RM; visualization, XTY and RM; supervision, XTY and RM; project administration, RD; funding acquisition, RD. All authors have read and agreed to the published version of the manuscript.

## Funding

This research was supported by the University of Strathclyde.

## Data availability

All data generated or analysed during this study are included in this published article.

## Code availability

The code is available by request.

## Declarations

### Conflict of interest

The authors declare no conflict of interest.

## Open Access

This article is licensed under a Creative Commons Attribution 4.0 International License, which permits use, sharing, adaptation, distribution and reproduction in any medium or format, as long as you give appropriate credit to the original author(s) and the source, provide a link to the Creative Commons licence, and indicate if changes were made. The images or other third party material in this article are included in the article's Creative Commons licence, unless indicated otherwise in a credit line to the material. If material is not included in the article's Creative Commons licence and your intended use is not permitted by statutory regulation or exceeds the permitted use, you will need to obtain permission directly from the copyright holder. To view a copy of this licence, visit http://creativecommons.org/licenses/by/4.0/.

## References

1. N. Tepylo, X. Huang, P.C. Patnaik, Laser-based additive manufacturing technologies for aerospace applications. Adv. Eng. Mater. **21**(11), 659–681 (2019). https://doi.org/10.1002/adem.201900617
2. D. Bourell et al., Materials for additive manufacturing. CIRP Ann. **66**(2), 659–681 (2017). https://doi.org/10.1016/j.cirp.2017.05.009
3. L.J. Tan, W. Zhu, K. Zhou, Development of organically modified montmorillonite/polypropylene composite powders for selective laser sintering. Powder Technol. **369**, 25–37 (2020). https://doi.org/10.1016/j.powtec.2020.05.005
4. R. Dogea, X.T. Yan, R. Millar, A smart wing rib structure suitable for design for additive manufacturing (DfAM) process. J. Mater. Sci. Manuf. Res. **2**(2), 1–21 (2021). https://doi.org/10.47363/jmsmr/2021(2)122
5. B. Blakey-Milner et al., Metal additive manufacturing in aerospace: a review. Mater. Des. **209**, 110008 (2021). https://doi.org/10.1016/j.matdes.2021.110008
6. Y. Ueda, H. Murakawa, and N. Ma, *Welding Deformation and Residual Stress Prevention*. 2012.
7. J. Baiges, M. Chiumenti, C.A. Moreira, M. Cervera, R. Codina, An adaptive finite element strategy for the numerical simulation of additive manufacturing processes. Addit. Manuf. **37**, 101650 (2021). https://doi.org/10.1016/j.addma.2020.101650
8. H. Alzyod, P. Ficzere, Using finite element analysis in the 3D printing of metals. Hungarian J. Ind. Chem. **49**(2), 65–70 (2021). https://doi.org/10.33927/hjic-2021-24
9. T. Mayer, G. Brändle, A. Schönenberger, R. Eberlein, Simulation and validation of residual deformations in additive manufacturing of metal parts. Heliyon **6**(5), e03987 (2020). https://doi.org/10.1016/j.heliyon.2020.e03987
10. R. Ghiaasiaan, S. Shankar, D. Apelian, Control diffusion solidification (CDS): an overview of mechanism and application, in *Shape casting: 5th international symposium 2014: shape/Tiryakioğlu*. ed. by M. Tiryakioğlu, J. Campbell, G. Byczynski (John Wiley & Sons Inc, NJ, 2014)
11. Q.L. Bai, Y. Li, H.X. Li, Q. Du, J.S. Zhang, L.Z. Zhuang, Roles of alloy composition and grain refinement on hot tearing susceptibility of 7××× aluminum alloys. Metall. Mater. Trans. A **47**(8), 4080–4091 (2016). https://doi.org/10.1007/s11661-016-3588-2
12. S. Afazov et al., Metal powder bed fusion process chains: an overview of modelling techniques. Prog. Addit. Manuf. **7**(2), 289–314 (2022). https://doi.org/10.1007/s40964-021-00230-1
13. D. Sang, R. Fu, Y. Li, The hot deformation activation energy of 7050 aluminum alloy under three different deformation modes. Metals (Basel) **6**(3), 49 (2016). https://doi.org/10.3390/met6030049
14. J.H. Zheng, R. Pan, C. Li, W. Zhang, J. Lin, C.M. Davies, Experimental investigation of multi-step stress-relaxation-ageing of 7050 aluminium alloy for different pre-strained conditions. Mater. Sci. Eng. A **710**, 111–120 (2018). https://doi.org/10.1016/j.msea.2017.10.066
15. S. Spigarelli, "Creep of Aluminium and Aluminium Alloys," *Talat*, 1999.
16. J.F. Chen, J.T. Jiang, L. Zhen, W.Z. Shao, Stress relaxation behavior of an Al-Zn-Mg-Cu alloy in simulated age-forming process. J. Mater. Process. Technol. **214**(4), 775–783 (2014). https://doi.org/10.1016/j.jmatprotec.2013.08.017
17. G. Chen, C. Ren, Z. Ke, J. Li, X. Yang, Modeling of flow behavior for 7050–T7451 aluminum alloy considering microstructural evolution over a wide range of strain rates. Mech. Mater. **95**, 146–157 (2016). https://doi.org/10.1016/j.mechmat.2016.01.006
18. S. Liu, J. You, X. Zhang, Y. Deng, Y. Yuan, Influence of cooling rate after homogenization on the flow behavior of aluminum alloy 7050 under hot compression. Mater. Sci. Eng. A **527**(4–5), 1200–1205 (2010). https://doi.org/10.1016/j.msea.2009.10.055
19. J. Li, F. Li, J. Cai, R. Wang, Z. Yuan, G. Ji, Comparative investigation on the modified Zerilli-Armstrong model and Arrhenius-type model to predict the elevated-temperature flow behaviour of 7050 aluminium alloy. Comput. Mater. Sci. **71**, 56–65 (2013). https://doi.org/10.1016/j.commatsci.2013.01.010
20. A. Singh, *Additive manufacturing Of Al 4047 and Al 7050 alloys using direct laser metal deposition process* (Wayne State University Dissertations, 2017)
21. ASM Metals Handbook, *ASM Handbook Vol. 2: Properties and selection--nonferrous alloys and special-purpose materials*, 2001.